# Catalysis Science & Technology

Accepted Manuscript






ROYAL SOCIETY OF CHEMISTRY

www.rsc.org/catalysis

# Fe-containing Polyimide-based High Performance ORR Catalysts in Acidic Medium: A Kinetic Approach to Study Durability of Catalysts

Azhagumuthu Muthukrishnan[1], Yuta Nabae[2], Teruaki Hayakawa[2], Takeyoshi Okajima[1], Takeo Ohsaka[1,*]

[1]Department of Electronic Chemistry, Interdisciplinary Graduate School of Science and Engineering, Tokyo Institute of Technology, G1-5, 4259 Nagatsuta, Midori-ku, Yokohama 226-8502, Japan.

[2]Department of Organic and Polymeric Materials, Graduate School of Science and Engineering, Tokyo Institute of Technology, 2-12-1, Ookayama, Megro-ku, Tokyo 152-8552, Japan.

*To whom correspondence should be addressed.

E-mail: ohsaka@echem.titech.ac.jp

Tel: +81-45-924-5404. Fax: +81-45-924-5489

Abstract

The ORR activity and durability of Fe-containing non-precious N-doped carbon catalysts was studied in acidic medium using a rotating ring-disk electrode voltammetry and XPS technique. The catalysts (Fe/PI) were synthesised from the pyrolysis of the $Fe(acac)_3$ and polyimide nanoparticle (PI) mixture. The catalytic activity and durability of Fe/PI is superior to the conventional phthalocyanine-based catalyst. The onset potential of ORR was 0.915 V vs. RHE in 0.5 M $H_2SO_4$ which is very close to that on a commercially available Pt/C catalyst. The Fe/PI catalyst sustains its activity and stability even after 11,110 repeating potential-steps between 0.6 and 1.0 V vs. RHE in $O_2$-saturated 0.5 M $H_2SO_4$ and 1,110 potential cycles between 1.0 and 1.5 V vs. RHE in argon-saturated 0.5 M $H_2SO_4$, respectively. The kinetic and mechanistic analyses of the ORR on this catalyst indicate that the ORR, as a whole, follows 4-electron (parallel) pathway. The N 1s XPS spectra before and after the durability test indicate that pyridinic and graphite-like nitrogens take part in improving the ORR activity, whereas nitrogen oxides have the negative role in the ORR. The loss of ORR activity was observed after the acid washing of the catalysts which suggests the role of Fe in the overall 4-electron reduction of $O_2$.

Keywords: Oxygen reduction reaction; Nitrogen-doped carbon; Rotating ring-disk electrode voltammetry; X-ray photoelectron spectroscopy; Electrode kinetics

1.Introduction

Recently, many researchers have focused on developing non-precious metal catalysts for the oxygen reduction reaction (ORR) in polymer electrolyte membrane fuel cells in order to overcome the cost and scarcity of the platinum and its alloy catalysts. Non-precious metal nitrogen-doped carbon catalysts have been proposed as the promising catalysts for this purpose[1-18]. The ORR activity of theses catalysts are sometimes found to be better than that of platinum-based catalysts in alkaline media, but they are inferior in ORR activity to the platinum-based catalysts in acidic media. Moreover, their metal-free catalysts are active only in alkaline media[17, 19-24]. Early studies were focused on the heat-treated transition metal macrocyclic complexes[25-28] and later, nitrogen-containing organic polymers, especially ployaniline (PANI) have been used as the precursors[29-32] for preparing the effective ORR catalysts. Recently, many researchers have confined their attention to the heat treatment of small nitrogen-containing organic molecules[33-41], and also to N-doped carbon nanotubes (NCNT) [4, 10, 42-46] and N-doped graphene (NGr)[11, 46-61] for obtaining the better ORR activity in acidic as well as alkaline media. In addition, our research group has recently reported a very active non-precious metal catalyst prepared from polyimide nano-particles[62], which is one of the catalysts exhibiting the best fuel cell performance in the world and can be prepared from ordinary chemicals, pyromellitic acid dianhydride (PMDA) and 4,4'-oxydianiline (ODA), which are the most common polyimide precursors.

Studying the kinetics of such highly active catalysts is very useful in understanding the mechanism of ORR and further improving the catalytic performance. A rotating ring-disc electrode voltammetry is often used to study the kinetics of the ORR. In general, the mechanism of ORR is considered to follow one of the two different reduction pathways or both of them during the reduction of $O_2$ to water as proposed by Damjanovic et al. (Scheme 1)[63]. The two pathways of ORR are the direct reduction involving 4-electron transfer (direct

pathway) and the stepwise reduction via $H_2O_2$ intermediate involving 2-electron transfer in each step (sequential pathway). This model was proposed with three assumptions: (a) no catalytic decomposition of $H_2O_2$, (b) adsorption-desorption of $H_2O_2$ is fast and in equilibrium and (c) re-oxidation of $H_2O_2$ is negligible.

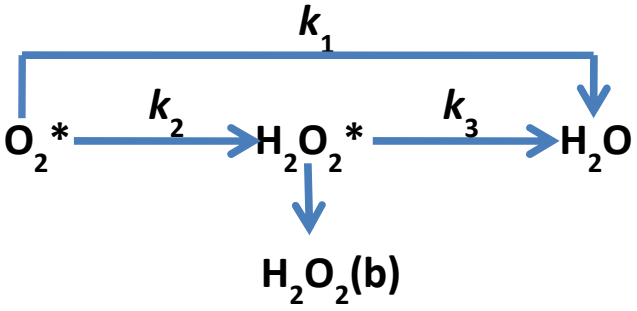


Scheme 1. Proposed model for the electrochemical reduction of $O_2$ by Damjanovic [63] et al. Indices b and * designate the bulk species and the species in the vicinity of the disk electrode, respectively.

In this work, using a rotating ring-disk electrode voltammetry, we have studied the ORR activity of the Fe/PI and acid-washed Fe/PI (hereafter designed as Fe/PI-aw) catalysts. Figure 1 shows the precursors for the Fe/PI catalyst: polyimide and $Fe(acac)_3$ as carbon-nitrogen and Fe sources, respectively. The effect of acid-washing of the Fe/PI catalyst on its durability and activity in ORR is examined. The durability of the catalysts is studied in two different modes of potential application by reference to those used in the durability test of Pt/C catalysts[64, 65]. Based on the individual rate constants of ORR ($k_1$, $k_2$ and $k_3$) estimated according to the Damjanovic model[63] before and after the durability test, the ORR performance and durability of Fe/PI and Fe/PI-aw catalysts are discussed. In addition, a possibility of the disproportionation reaction of $H_2O_2$ catalysed by the porous Fe/PI and Fe/PI-aw catalysts is also discussed.

## 2. Experimental

### 2.1 Preparation of Fe-containing polyimide catalyst (Fe/PI)

Fe/PI was prepared according to the recently reported procedure[62]. A solution of pyromellitic acid dianhydride (PMDA) in acetone was added to a solution of 4,4'-oxydianiline (ODA) and tris(acetylacetonato) iron(III) ($Fe(acac)_3$, >98.0%, Dojindo) in acetone (>99.0 %, Wako). The amount of Fe species was 2 wt% with relative to the resulting polyimide. The mixture was stirred at 0 ˚C for 30 min and the solvent was removed with a rotary evaporator to collect poly(amic acid). The curing reaction was conducted by heating the poly(amic acid) at 200˚C under vacuum to obtain fine particles of polyimide. The thus-obtained composite was converted into Fe/PI by the multi-step pyrolysis[66]. The precursor was heated at 600° C at nitrogen atmosphere for 5 hrs and washed with conc. HCl. And then, the product was again heated at 800° C in ammonia atmosphere for one hour and washed with conc. HCl. Finally, it was further heated at 1000° C under ammonia atmosphere for one hour to obtain Fe/PI. Fe/PI-aw was prepared by washing Fe/PI with conc. HCl.

2.2 Preparation of Fe/PI-modified GC electrodes

The composition and coating of the Fe/PI ink play an important role in preparing a uniform thin layer of the Fe/PI on the GC electrode surface. 5 mg of each Fe/PI was weighed into a 1 ml bottle followed by the addition of 150 µl of ethanol, 150 µl of milli Q-water (18.2 MΩ) and 50 µl of the 5 wt% Nafion. This mixture was sonicated in the ice-cold water bath for one hour. 4 µl of the uniform by dispersed ink was taken using micropipette and transferred onto the clean, polished GC disk electrode and the whole surface of the GC disk electrode was covered by the ink with a uniform thickness. (*Care must be taken that the ink should cover the GC disk of rotating ring-disk electrode completely and it should not flow into the Teflon gap between the ring and disk electrodes*) The electrode was then dried under low flow of argon environment until it dried completely. The thus-prepared Fe/PI–modified GC electrodes contained 0.2 mg $cm^{-2}$ of Fe/PI with 0.1 mg $cm^{-2}$ of the Nafion binder.

2.3 Electrochemical measurements

All the measurements were carried out in 0.5 M $H_2SO_4$ using a CHI bi-potentiostat (model 700D) in the custom-built electrochemical cell. The rotating ring-disk electrode (RRDE) with GC disk (6 mm in diameter, 0.283 $cm^2$) and Pt ring (0.252 $cm^2$), carbon plate (~ 7 $cm^2$) and Ag/AgCl (sat. KCl) were used as working, counter and reference electrodes, respectively. The working electrode was polished with 1 μ and 0.06 μ alumina power to mirror finish and sonicated to remove the alumina particles before each experiment. After the disk electrode was modified with each Fe/PI, its surface was wetted with 0.5 M $H_2SO_4$ completely without any air-droplets on the surface. The pretreatment of the Fe/PI-modified GC disk electrode was carried out by repeating potential scan at 0.05 $Vs^{-1}$ between 1.1 and 0.05 V in argon–saturated 0.5 M $H_2SO_4$ until stable voltammograms were obtained. Similarly, the Pt ring electrode was also treated by potential scanning at 0.05 $Vs^{-1}$ between the onset potential of hydrogen evolution (ca. 0 V) and 1.2 V until a voltammogram characteristic of clean Pt electrode was obtained. The thus-pretreated electrodes were used to study the ORR by scanning the disk electrode potential from 1.1 to 0.05 V in $O_2$–saturated 0.5 M $H_2SO_4$ at a scan rate of 5 $mVs^{-1}$ at various electrode rotation speeds of 400 to 3600 rpm. At the same time the Pt ring electrode was polarized at a constant potential of 1.2 V to measure the amount of $H_2O_2$ formed during the ORR at the disk electrode (The collection efficiency is 0.37). The blank response was also measured in argon–saturated 0.5 M $H_2SO_4$ at the same experimental conditions used above. Electrode potential was finally corrected to a reversible hydrogen electrode (RHE) by adding 0.227 V, estimated from the pH of the 0.5 M $H_2SO_4$, to the electrode potential measured against Ag/AgCl (sat. KCl). Unless otherwise mentioned, the potentials in this article are referred to a RHE.

The durability or stability test of the Fe/PI was carried out in two different modes of potential application: the stability of the "carbon support" in the Fe/PI was tested using the

protocol based on the potential cycling between (typically using 10, 110 and 1,110 cycles) 1.0 and 1.5 V at a scan rate of 0.5 $Vs^{-1}$ in argon–saturated 0.5 M $H_2SO_4$. On the other hand, the stability in the Fe/PI' ORR activity was tested by repeating the potential step between ORR-off region (1.0 V for 3 s) and ORR-on region (0.6 V for 3 s) for 11,110 times (max). Hereafter, the former and latter durability tests will be called as start-stop durability (SSD) test and loading durability (LD) test, respectively[64, 65].

2.4 XPS measurements

For XPS measurements, the Fe/PI samples, which were prepared by the similar coating procedure used in the preparation of Fe/PI-modified GC disk electrodes for their electrochemical measurements, were placed under an ultra-high vacuum condition ($10^{-6}$ Pa) where an ESCA3400 electron spectrometer (SHIMADZU) with unmonochromatized X-ray source [MgKa (hν=1253.6eV) anode, emission current of 20 mA and acceleration voltage of 10 kV] was employed, operating at 200 W. The photoelectron take-off angle was set to 75°, the analyzer pass energy was set to 75 eV, and the XPS spectra were corrected to the internal reference spectra of C 1s at 284.5 eV, being the binding energy of the C=C bond of the GC substrate, in order to compensate the electrostatic charging. Then, the core level spectra were carefully deconvoluted to investigate the different nitrogen species, i.e., pyridinic nitrogen, pyrrolic nitrogen, graphite-like nitrogen and nitrogen oxide on the Fe/PI and Fe/PI-aw surfaces. The XPS spectra of the N core levels were fitted with partial Gaussian functions (usually around 50-80% and the rest being Lorentzian).

3. Results and Discussion

3.1 XPS analysis

Figure 2 shows the N 1s XPS spectra of the Fe/PI and Fe/PI-aw before and after the LD test (11,110 potential steps). The N 1s spectra were carefully deconvoluted to investigate the chemical state of nitrogen in these catalysts. Four common nitrogen groups observed in nitrogen-containing carbonaceous materials are pyridinic nitrogen (Py-N), pyrrolic nitrogen (Pr-N), graphite-like nitrogen (Q-N) and nitrogen oxide (N-O), the peaks of which were observed in the regions of 398.2 - 398.7, 400.1 – 400.3, 401.5 – 401.2 and 402.2 – 403.1 eV, respectively[67]. The percentage of each kind of nitrogens can be calculated from the corresponding peak area before and after the LD test (Table 1). Previous studies suggest that the Py-N and Q-N improve the ORR activity[68-70] whereas the N-O shows a negative effect on the ORR. In this study, we have found that the amount of Py-N and Q-N is 22 and 27%, respectively, for the Fe/PI catalyst, whereas in the Fe/PI-aw catalyst, the quantity of Py-N and Q-N decreases to 0 and 21%, respectively, This observation indicates that the acid-washed catalyst did not render high ORR activity compared with the non-washed one. Moreover, the amount of N-O is abnormally high in the Fe/PI-aw catalyst (48%) also supporting a poor activity of the acid-washed catalyst towards the ORR. However, the situation changes after the durability test of Fe/PI-aw catalyst, that is, after the 11,110 durability cycles the relative amount of Py-N and Q-N increases, while the N-O amount decreases considerably, being in agreement with the increasing activity of the Fe/PI-aw catalyst towards the ORR after the durability test (see the inset in Fig. 5B). The each quantity of the nitrogen species before and after the durability test of 11,110 potential-steps remains almost unchanged for the Fe/PI catalyst reflecting a high stability towards the ORR. The relative quantity of Pr-N of the both catalysts decreases by ca. 2% after the durability test. The XPS peak found at 711 eV for the Fe/PI corresponds to the Fe-$2p_{3/2}$, but this peak was not observed for the Fe/PI-aw. This confirmed the removal of iron from the catalyst by the acid-washing.

3. 2 Rotating ring-disk electrode voltammetry

The RRDE voltammograms obtained for Fe/PI and Fe/PI-aw catalysts (before the durability test) at 1600 rpm in $O_2$–saturated 0.5 M $H_2SO_4$ are shown in Figure 3A. The onset potential ($E_{onset}$) of the ORR was measured as a potential at which the disk current reaches 10 μA $cm^{-2}$. The Fe/PI catalyst exhibits a fairly positive $E_{onset}$ (0.915 V) which is by ~100 mV more negative than that at the commercially available Pt/C catalyst (TEC 10E50E (46 wt% Pt, purchased from Tanaka Kikinzoku Kogyo Corp., Japan (TKK)) with the loading density of 55.8 $\mu g_{Pt}$ $cm^{-2}$ and the Fe/PI-aw shows a little negative shift in $E_{onset}$ (0.902 V). The half-wave potential ($E_{1/2}$) obtained at the Fe/PI-aw (0.724 V) was found to be more negative than that at the Fe/PI (0.751). The limiting current density ($i_{DL}$) obtained at the Fe/PI is close to that obtained at the Pt/C. A little decrease in the $i_{DL}$ was observed for the acid-washed catalyst

3.3 Number of electrons and percentage of hydrogen peroxide

The background-subtracted RRDE voltammograms were used for the estimation of potential-dependent parameters of ORR such as the number of electrons ($n$), the percentage of hydrogen peroxide produced ($\chi H_2O_2$) and the rate constants. The estimation of $n$ in the kinetically controlled region helps us to identify the reaction pathway for the reduction of oxygen to water as described in Scheme 1. The value of $n$ can be estimated using the ring and disc currents as follows[71-74],

$$n = \frac{4I_D}{I_D + \frac{I_R}{N}} \qquad (1)$$

where $I_D$ and $I_R$ represent the disk and ring currents, respectively. $N$ is the collection efficiency (in this case 0.37). Similarly, $\chi H_2O_2$ is also estimated using the following equation[71-74]:

$$\chi_{H_2O_2} = \frac{\frac{2I_R}{N}}{I_D + \left(\frac{I_R}{N}\right)} \quad (2)$$

Potential-dependent variation in *n* and $\chi H_2O_2$ is shown in Figure 3B. The *n* increases as the electrode potential becomes more negative and at the limiting current region, its values are 3.8 to 3.95 (depending on the catalysts) which are very close to that expected for 4-electron reduction of oxygen to water. The percentage of $H_2O_2$ increases as the potential becomes more positive and the value is ~20% in the ORR onset region whereas at the limiting current region, it is less than 5%, indicating that the ORR actually follows both a direct pathway of the 4-electron reduction of $O_2$ to $H_2O$ and a sequential pathway, where $O_2$ is first reduced to $H_2O_2$ followed by the reduction of $H_2O_2$ to $H_2O$, rather than only either of both, i.e., a parallel pathway (Scheme 1).

3.4 Stability tests

3.4.1 Stability of the carbon support

The stability test of the Fe/PI as "carbon support" was carried out at the potential region where carbon corrosion may occur using the protocol (*i.e.,* SSD test) described in the Experimental section. The $E_{1/2}$ and $I_{DL}$ are the two important parameters reflecting the stability of Fe/PI. The $E_{1/2}$ is shifted to the negative direction of potential after the stability test (the degree in $E_{1/2}$ shift is noted by the difference in $E_{1/2}$ ($\Delta E_{1/2}$) before and after the stability test) and the $\Delta E_{1/2}$ values for the Fe/PI and Fe/PI-aw catalysts are 40 and 60 mV, respectively. The decreased $I_{DL}$ after the SSD test is attributed to the leaching of the ORR active sites from the electrode surface, probably resulting from the carbon corrosion of the Fe/PI. The difference in $i_{DL}$ before and after the stability test was found to be within 5%.

3.4.2 Stability of Fe/PI catalyst in its ORR activity

The stability in the Fe/PI' ORR activity was also examined by applying the potential-step protocol (*i.e.,* LD test) as mentioned in the Experimental section. In this study, the potential-step was repeated for 11,110 times (max.) and the ORR performances of the individual catalysts were checked at the $10^{th}$, $110^{th}$, $1{,}110^{th}$ and $11{,}110^{th}$ steps using the RRDE voltammetry and the results are shown in Figure 4. The negative shift of $E_{1/2}$ was observed after the LD test as in the case of the SSD test. This shift increased with increasing the number of the potential-step and was 36 mV after the 11,110 potential-steps. No appreciable changes were observed in $E_{onset}$ and $I_{DL}$. However, the $n$ and $\chi H_2O_2$ decreased and increased, respectively, with increasing the number of potential-step. The values of $n$ and $\chi H_2O_2$ (%) before the LD test were found to be, for example, approximately 3.9 and 6% (at 0 V), respectively, whereas they did not change so much after 11,110 LD potential-steps. In the case of the Fe/PI-aw, the values of $n$ and $\chi H_2O_2$ (%) before and after the LD test are found to be approximately 3.8 and 11%, respectively, at 0 V.

3.5 Kinetics and mechanism of ORR

To study the kinetics and mechanism of the ORR, the analytical procedure based on a RRDE voltammetry on the ORR (Scheme 1), which was originally given by Damjanovic et al.[63] and later developed by Hsueh et al.[75], was used in this study. The individual rate constants ($k_1$, $k_2$ and $k_3$) were estimated from the slopes and intercepts of the $I_D/I_R$ vs. $\omega^{-1/2}$ and $I_{DL}/(I_{DL}-I_D)$ vs. $\omega^{-1/2}$ plots where $I_{DL}$ and $\omega$ are the limiting disk current and rotational speed, respectively. The plots of $I_{DL}/(I_{DL}-I_D)$ vs. $\omega^{-1/2}$ at various potentials indicated a liner behaviour with an intercept equal to unity, suggesting that the decomposition (i.e., disproportionation) of the intermediate $H_2O_2$ formed during the ORR is negligible. The catalytic decomposition of the $H_2O_2$ on the surface of the catalysts has been also studied

separately as shown later. Following the procedure of Hsueh et al., the individual rate constants are calculated using the following equations[75]

$$k_1 = S_2 Z_1 \frac{I_1 N - 1}{I_1 N + 1}, \qquad k_2 = \frac{2 Z_1 S_2}{I_1 N + 1} \quad \text{and} \quad k_3 = \frac{Z_2 N S_1}{I_1 N + 1} \tag{3}$$

where $S_1$ and $I_1$ are the slope and intercept of the $I_D/I_R$ vs. $\omega^{-1/2}$ plot, respectively and $S_2$ indicates the slope of $I_{DL}/(I_{DL}\text{-}I_D)$ vs. $\omega^{-1/2}$ plot. $Z_1 = 0.62 D_{O_2}^{2/3} v^{-1/6}$ and $Z_2 = 0.62 D_{H_2O_2}^{2/3} v^{-1/6}$ with the values of $D_{O_2} = 1.4 \times 10^{-5} \mathrm{cm^2 s^{-1}}$, $D_{H_2O_2} = 6.8 \times 10^{-6} \mathrm{cm^2 s^{-1}}$ and $v = 0.01\ \mathrm{cm^2 s^{-1}}$ [76]. The estimated rate constants in the potential range from 0.75 to 0.4 V are shown typically in Figure 5A and 5B for the catalysts Fe/PI and Fe/PI-aw, respectively. The rate constants $k_1$ and $k_2$ are the same potential-dependent while the $k_3$ is almost potential-independent. The ratios of $k_1/k_2$ are much larger than unity in the examined range of potential for the Fe/PI catalyst (0.4-0.7 V), i.e., 5.5-8.3 and 4-7.5 before and after the LD test, respectively (the inset in Figure 5A), indicating that $O_2$ is mainly reduced to $H_2O$ via the 4-electron reduction path and only trace amounts of $O_2$ are reduced via the sequential path which involves $H_2O_2$ as an intermediate. Similarly, the Fe/PI-aw shows the ratios of $k_1/k_2$ larger than unity, but after the durability test the ratios are increased from ca. 2~3 to ca. 4~7.5, i.e., the 4-electron reduction is facilitated (cf. the inset in Figure 5B). The $k_1/k_2$ ratios are almost linearly dependent on potential and the values are smaller at more positive potential. The rate constant $k_3$ is smaller than $k_2$. This indicates that the intermediate $H_2O_2$ formed in the sequential path is reduced to $H_2O$ at a relatively slow rate. The similar behaviour has been also reported for the Mo-Ru-Se based electrocatalyst for ORR[76].

As discussed in Section 3.4.2, a negative shift of $E_{1/2}$, a decrease in $n$ and an increase in $H_2O_2$ generation were observed after the durability test. These preliminary observations indicate that the electrode kinetics of the ORR becomes more sluggish after the durability test. An appreciable decrease in $k_1$ was observed for the Fe/PI, typically 42%. The similar trend

was observed for $k_2$ and $k_3$, but the extent of decrease was not as high as $k_1$. On the other hand, interestingly, the rate constants were found to increase after the durability test for the Fe/PI-aw, although this remains to be clarified. Furthermore, the Fe/PI-aw showed a less stability compared with the Fe/PI.

### 3.6 Disproportionation of $H_2O_2$

It is important in clarifying the overall ORR mechanism to know the catalytic decomposition of the $H_2O_2$ intermediate formed during the ORR. In the above-mentioned kinetic analysis, based on the fact that $I_{DL}/(I_{DL}-I_D)$ vs. $\omega^{-1/2}$ plots are linear with the intercept of unity, we have considered that the disproportionation of $H_2O_2$ on the catalyst surface is negligible. This was confirmed actually by estimating the disproportionation rate constants in the presence of Fe/PI or Fe/PI-aw according to the procedure proposed by Jaouen and Dodelet[77]. A known amount (2 mg) of each of the catalysts was added to the known volume (50 mL) of $O_2$-saturated 0.1 M $HClO_4$ and the solution was stirred with a uniform distribution of the catalyst. 51.1 μL of 30% $H_2O_2$ was added to the solution, resulting in an initial $H_2O_2$ concentration of 10 mM. Immediately after addition of $H_2O_2$, the RRDE voltammetric diffusion-limitted current ($I_{DL,t}$) was measured at constant intervals with the Pt/C electrode (the loading density of the Pt/C electrode is 37.2 μg/cm$^2$) at 1600 rpm rotational speed. The RRDE voltammogram was also measured before the addition of $H_2O_2$ in the $O_2$-saturated solution and the obtained time-independent current limited by $O_2$ diffusion is mentioned as $I_{DL,O2}$. Finally, the time-dependent $H_2O_2$ diffusion-limited current ($I_{DL,H2O2}$) was calculated as follows

$$I_{DL,H2O2} = I_{DL,t} - I_{DL,O2} \qquad (4)$$

The rate constants ($k_4$) of the homogeneous disproportionation reaction of $H_2O_2$ can be calculated from log($I_{DL,H2O2}$) vs. time plots as shown in Figure 6. The slopes for the both catalysts gave the values of $k_4$.

To compare the thus-estimated disproportionation rate constants with the ORR rate constants, the unit (cm $s^{-1}$) of $k_1$, $k_2$ and $k_3$ needs to be converted to the same unit of the homogenous rate constant ($k_4$) by taking into account the thickness ($l$) of the catalyst coated on the electrode. The ORR rate constants divided by the thickness of the film leads to the unit of $s^{-1}$ as shown in the Appendix-A. The thickness of the film coated on the GC surface was estimated as 23±3 μm using 3D leaser Scanning Microscope (Keyence Co., Japan). Finally, the $k_1/l$, $k_2/l$ and $k_3/l$ are calculated as 104.3, 12.0 and 1.2 $s^{-1}$, respectively, for the Fe/PI and 26.1, 9.4 and 1.4 $s^{-1}$, respectively, for the Fe/PI-aw catalyst. The $k_4$ is normalized to the amount of the catalyst coated on the electrode for the comparison and the estimated values are $4.1\times10^{-5}$ and $3.3\times10^{-5}$ $s^{-1}$ for the Fe/PI and Fe/PI-aw, respectively. These values are very low compared with the $k_1/l$, $k_2/l$ and $k_3/l$ and hence the disproportionation of $H_2O_2$ is negligible. From the mechanistic point of view it is expected that $k_4$ might influence on $k_3$, but not on $k_1$ and $k_2$ [75]. As mentioned above, $k_4$ is too small compared to the $k_3$. Hence the catalytic disproportionation reaction of $H_2O_2$ on these catalysts is considered to be very slow and it is negligible.

3.6 Tafel analysis

Tafel plots are very useful in examining the mechanism of ORR on a particular catalyst. For estimating the kinetic current to obtain the mass transfer–corrected Tafel plot, the modified Koutecky-Levich equation was used as shown below,

$$\frac{1}{i_k} = \frac{i_{DL} i_D}{i_{DL} - i_D} \qquad (7)$$

where $i_k$ and $i_{DL}$ is the kinetic and limiting current densities, respectively. The estimated $i_k$ values are plotted against potential in Figure 7. For both Fe/PI and Fe/PI-aw catalysts the good linear plots were obtained and thus the Tafel slopes were estimated to be -66 and -65 mV $dec^{-1}$ for Fe/PI and Fe/PI-aw catalysts, respectively. It is well recognized for Pt/C catalysts [73, 78-80] that the slope of -60 mV $dec^{-1}$ is expected for the ORR at low current density (*lcd*) region and it is attributed to the adsorbed oxygen species with the fast initial electron transfer step followed by the rate-determining chemical step or adsorption under the Temkin adsorption condition and larger values of Tafel slopes (from ca. -120 to -160 mV $dec^{-1}$) are obtained usually at high current density (*hcd*) region in agreement with the expectation that the initial electron transfer is the rate-determining step under the Langmuir adsorption condition. The exchange current density ($I_{ex}$) can be estimated from the intercept of a linear Tafel plot and it is a key parameter to judge the catalytic efficiency. For the Pt/C these values were estimated to be $3.9x10^{-8}$ and $3.9x10^{-5}$ A $cm^{-2}$ for *lcd* and *hcd* regions, respectively. The $I_{ex}$ values obtained for the Fe/PI and Fe/PI-aw are $1.1\times10^{-10}$ and $4.6\times10^{-11}$ A $cm^{-2}$, respectively, which are by two-three order of magnitude smaller than that at *lcd* foe the Pt/C. The Fe/PI catalyst gives a larger $I_{ex}$ compared with the Fe/PI-aw.

## 4. Conclusions

In conclusion, we have successfully demonstrated the high performance of Fe-containing N-doped carbon catalyst (Fe/PI) for the ORR in acidic medium. The Fe/PI was prepared from the high temperature pyrolysis of the polyimide precursor with the $Fe(acac)_3$. The durability of the Fe/PI, which was estimated based on the SSD and LD tests, is relatively good in acidic medium compared with other catalysts reported in the literature[16, 81-83]. The XPS and RRDE results suggested that the catalyst enriched with Py-N and Q-N shows a high activity towards the ORR, while that enriched with N-O shows a less activity. The ORR rate constants ($k_1$, $k_2$ and $k_3$) were estimated by a RRD voltammetry, indicating that the 4-electron

reduction of oxygen is relatively predominant compared to the 2-electron reduction. The rate constant of the disproportionation reaction of $H_2O_2$ was estimated; it is by about 4 to 6 orders of magnitude smaller than the ORR rate constants and hence, in the present case, the disproportionation reaction is negligible actually. The role of iron was also studied by comparing the activity and durability in ORR of the Fe/PI and Fe/PI-aw catalysts. Its role in the catalytic performance is not known exactly, but it seems true that the Fe plays a vital function in the overall 4-electron reduction of $O_2$.

Acknowledgments

This work was financially supported by the New Energy and Industrial Technology Development Organization (NEDO), Japan. The authors thank Dr. T. Fuchigami and Dr. D. Zhang for helpful discussions.

Appendix-A

According to the definition of the Damjanovic model, the current corresponding to the reduction of $H_2O_2$ to water ($I_3$) can be represented as

$$I_3 = 2S_D F k_3 C_2^* \qquad (A1)$$

where $S_D$, $F$ and $C_2^*$ represent the surface area of the disk electrode, Faraday constant and the concentration of $H_2O_2$, respectively. The rate of the reduction of $H_2O_2$ is also defined as

$$r_3 = \frac{I_3}{2FV} \qquad (A2)$$

Substituting Eq ($A1$) to Eq ($A2$),

$$r_3(mol\ cm^3 s^{-1}) = \frac{k_3 C_2^*}{l} \qquad (A3)$$

where $l$ is the thickness of the electrode evolved from the ratio of the surface area to the volume of the electrode. The rate of the disproportionation reaction of $H_2O_2$ ($r_4$) can be written as

$$r_4(mol\ cm^3 s^{-1}) = k_4 \left(\frac{w_{cat}}{m}\right) C_2^* \qquad (A4)$$

where $k_4$ is the homogeneous disproportionation rate constant ($s^{-1}$), $w_{cat}$ and $m$ are the weight of the catalyst on the electrode surface in the ORR study and the weight of the catalyst used for the disproportionation study (2 mg), respectively. By taking $k_4^* = k_4 \left(\frac{w_{cat}}{m}\right)$, $k_4^*$ can be compared with the $k_3/l$. Similarly, the $k_1/l$ and $k_2/l$ are also compared with $k_4^*$.

References


1. S. Gupta, D. Tryk, I. Bae, W. Aldred and E. Yeager, *J. Appl. Electrochem.*, 1989, 19, 19-27.
2. F. Jaouen, S. Marcotte, J.-P. Dodelet and G. Lindbergh, *J. Phys. Chem. B*, 2003, 107, 1376-1386.
3. M. Lefevre, E. Proietti, F. Jaouen and J.-P. Dodelet, *Science (Washington, DC, U. S.)*, 2009, 324, 71-74.
4. S. Kundu, T. C. Nagaiah, W. Xia, Y. Wang, S. Van Dommele, J. H. Bitter, M. Santa, G. Grundmeier, M. Bron, W. Schuhmann and M. Muhler, *J. Phys. Chem. C*, 2009, 113, 14302-14310.
5. T. C. Nagaiah, S. Kundu, M. Bron, M. Muhler and W. Schuhmann, *Electrochem. Commun.*, 2010, 12, 338-341.
6. G. Wu, K. L. More, C. M. Johnston and P. Zelenay, *Science (Washington, DC, U. S.)*, 2011, 332, 443-447.
7. G. Wu, K. L. More, P. Xu, H.-L. Wang, M. Ferrandon, A. J. Kropf, D. J. Myers, S. Ma, C. M. Johnston and P. Zelenay, *Chem. Commun. (Cambridge, U. K.)*, 2013, 49, 3291-3293.
8. Z. Chen, D. Higgins and Z.-W. Chen, *Electrochim. Acta*, 2010, 55, 4799-4804.
9. Z. Chen, D. Higgins, H. Tao, R. S. Hsu and Z. Chen, *J. Phys. Chem. C*, 2009, 113, 21008-21013.
10. K. Gong, F. Du, Z. Xia, M. Durstock and L. Dai, *Science (Washington, DC, U. S.)*, 2009, 323, 760-764.
11. L. Qu, Y. Liu, J.-B. Baek and L. Dai, *ACS Nano*, 2010, 4, 1321-1326.
12. M. Chokai, M. Taniguchi, S. Moriya, K. Matsubayashi, T. Shinoda, Y. Nabae, S. Kuroki, T. Hayakawa, M.-a. Kakimoto, J.-i. Ozaki and S. Miyata, *Journal of Power Sources*, 2010, 195, 5947-5951.
13. J.-i. Ozaki, S.-i. Tanifuji, A. Furuichi and K. Yabutsuka, *Electrochimica Acta*, 2010, 55, 1864-1871.
14. G. Ma, R. Jia, J. Zhao, Z. Wang, C. Song, S. Jia and Z. Zhu, *J. Phys. Chem. C*, 2011, 115, 25148-25154.

15. M. H. Robson, A. Serov, K. Artyushkova and P. Atanassov, *Electrochimica Acta*, 2013, 90, 656-665.
16. H. Peng, Z. Mo, S. Liao, H. Liang, L. Yang, F. Luo, H. Song, Y. Zhong and B. Zhang, *Scientific reports*, 2013, 3.
17. L. Qu, Y. Liu, J.-B. Baek and L. Dai, *ACS nano*, 2010, 4, 1321-1326.
18. H. Niwa, M. Saito, M. Kobayashi, Y. Harada, M. Oshima, S. Moriya, K. Matsubayashi, Y. Nabae, S. Kuroki, T. Ikeda, K. Terakura, J.-i. Ozaki and S. Miyata, *Journal of Power Sources*, 2013, 223, 30-35.
19. Y. Gong, S. Yang and P. Ajayan, 2014.
20. S.-Y. Wang, D.-S. Yu, L.-M. Dai, D.-W. Chang and J.-B. Baek, *ACS Nano*, 2011, 5, 6202-6209.
21. X. Zhou, J. Qiao, L. Yang and J. Zhang, *Adv. Energy Mater.*, 2014, 4, 1301523/1301521-1301523/1301525.
22. Z.-W. Liu, F. Peng, H.-J. Wang, H. Yu, W.-X. Zheng and J. Yang, *Angew. Chem., Int. Ed.*, 2011, 50, 3257-3261, S3257/3251-S3257/3212.
23. Y. Li, Y. Zhao, H. Cheng, Y. Hu, G. Shi, L. Dai and L. Qu, *J. Am. Chem. Soc.*, 2012, 134, 15-18.
24. X. Bo and L. Guo, *Phys Chem Chem Phys*, 2013, 15, 2459-2465.
25. K. Wiesener, D. Ohms, V. Neumann and R. Franke, *Mater. Chem. Phys.*, 1989, 22, 457-475.
26. K. A. Radyushkina and M. R. Tarasevich, *Elektrokhimiya*, 1986, 22, 1155-1170.
27. H. Meng, N. Larouche, M. Lefevre, F. Jaouen, B. Stansfield and J.-P. Dodelet, *Electrochim. Acta*, 2010, 55, 6450-6461.
28. J. A. R. Van Veen, J. F. Van Baar and K. J. Kroese, *J. Chem. Soc., Faraday Trans. 1*, 1981, 77, 2827-2843.
29. G. Wu, K. Artyushkova, M. Ferrandon, A. J. Kropf, D. Myers and P. Zelenay, *ECS Transactions*, 2009, 25, 1299-1311.
30. G. Wu, K. L. More, C. M. Johnston and P. Zelenay, *Science*, 2011, 332, 443-447.
31. N. Gavrilov, M. Vujkovic, I. A. Pasti, G. Ciric-Marjanovic and S. V. Mentus, *Electrochim. Acta*, 2011, 56, 9197-9202.
32. J. Chlistunoff, *J. Phys. Chem. C*, 2011, 115, 6496-6507.
33. S. Maldonado and K. J. Stevenson, *J. Phys. Chem. B*, 2005, 109, 4707-4716.
34. P. H. Matter, E. Wang, M. Arias, E. J. Biddinger and U. S. Ozkan, *J. Phys. Chem. B*, 2006, 110, 18374-18384.
35. S. Shanmugam and T. Osaka, *Chem. Commun. (Cambridge, U. K.)*, 2011, 47, 4463-4465.
36. J. Tian, L. Birry, F. Jaouen and J. P. Dodelet, *Electrochim. Acta*, 2011, 56, 3276-3285.
37. W. Yang, T.-P. Fellinger and M. Antonietti, *J. Am. Chem. Soc.*, 2011, 133, 206-209.
38. H. Jiang, Y. Zhu, Q. Feng, Y. Su, X. Yang and C. Li, *Chem. - Eur. J.*, 2014, 20, 3106-3112.
39. G. Nam, J. Park, S. T. Kim, D.-b. Shin, N. Park, Y. Kim, J.-S. Lee and J. Cho, *Nano Lett.*, 2014, 14, 1870-1876.
40. W. Wei, H. Liang, K. Parvez, X. Zhuang, X. Feng and K. Muellen, *Angew. Chem., Int. Ed.*, 2014, 53, 1570-1574.
41. R. Zheng, Z. Mo, S. Liao, H. Song, Z. Fu and P. Huang, *Carbon*, 2014, 69, 132-141.
42. Z. Chen, D. Higgins and Z. Chen, *Carbon*, 2010, 48, 3057-3065.
43. D. Yu, Q. Zhang and L. Dai, *J. Am. Chem. Soc.*, 2010, 132, 15127-15129.
44. D. Yu, Y. Xue and L. Dai, *J. Phys. Chem. Lett.*, 2012, 3, 2863-2870.
45. H. T. Chung, J. H. Won and P. Zelenay, *Nat. Commun.*, 2013, 4, ncomms2944, 2945 pp.
46. S. Ratso, I. Kruusenberg, M. Vikkisk, U. Joost, E. Shulga, I. Kink, T. Kallio and K. Tammeveski, *Carbon*, 2014, 73, 361-370.
47. I.-Y. Jeon, D. Yu, S.-Y. Bae, H.-J. Choi, D. W. Chang, L. Dai and J.-B. Baek, *Chemistry of Materials*, 2011, 23, 3987-3992.
48. P. Xu, D. Wu, L. Wan, P. Hu and R. Liu, *J. Colloid Interface Sci.*, 2014, 421, 160-164.
49. M. Vikkisk, I. Kruusenberg, U. Joost, E. Shulga, I. Kink and K. Tammeveski, *Appl. Catal., B*, 2014, 147, 369-376.

50. C. He, J. J. Zhang and P. K. Shen, *J. Mater. Chem. A*, 2014, 2, 3231-3236.
51. X. Bo, C. Han, Y. Zhang and L. Guo, *ACS Appl. Mater. Interfaces*, 2014, 6, 3013-3020.
52. Y. Jiang, Y. Lu, X. Lv, D. Han, Q. Zhang, L. Niu and W. Chen, *ACS Catalysis*, 2013, 3, 1263-1271.
53. J. Bai, Q. Zhu, Z. Lv, H. Dong, J. Yu and L. Dong, *International Journal of Hydrogen Energy*, 2013, 38, 1413-1418.
54. Z. Yang, Z. Yao, G. Li, G. Fang, H. Nie, Z. Liu, X. Zhou, X. a. Chen and S. Huang, *ACS Nano*, 2012, 6, 205-211.
55. S. Yang, L. Zhi, K. Tang, X. Feng, J. Maier and K. Muellen, *Adv. Funct. Mater.*, 2012, 22, 3634-3640, S3634/3631-S3634/3636.
56. G. Wu, N. H. Mack, W. Gao, S. Ma, R. Zhong, J. Han, J. K. Baldwin and P. Zelenay, *ACS Nano*, 2012, 6, 9764-9776.
57. K. Parvez, S. Yang, Y. Hernandez, A. Winter, A. Turchanin, X. Feng and K. Müllen, *ACS Nano*, 2012, 6, 9541-9550.
58. G. Wu, H. T. Chung, M. Nelson, K. Artyushkova, K. L. More, C. M. Johnston and P. Zelenay, *ECS Trans.*, 2011, 41, 1709-1717.
59. Z. Luo, S. Lim, Z. Tian, J. Shang, L. Lai, B. MacDonald, C. Fu, Z. Shen, T. Yu and J. Lin, *Journal of Materials Chemistry*, 2011, 21, 8038-8044.
60. Y. Liang, Y. Li, H. Wang, J. Zhou, J. Wang, T. Regier and H. Dai, *Nat Mater*, 2011, 10, 780-786.
61. Y. Li, Y. Zhao, H. Cheng, Y. Hu, G. Shi, L. Dai and L. Qu, *Journal of the American Chemical Society*, 2011, 134, 15-18.
62. Y. Nabae, Y. Kuang, M. Chokai, T. Ichihara, A. Isoda, T. Hayakawa and T. Aoki, *Journal of Materials Chemistry A*, 2014.
63. A. Damjanovic, M. A. Genshaw and J. O. M. Bockris, *J. Chem. Phys.*, 1966, 45, 4057-4059.
64. A. Ohma, K. Shinohara, A. Iiyama, T. Yoshida and A. Daimaru, *ECS Transactions*, 2011, 41, 775-784.
65. H. Yano, T. Akiyama, P. Bele, H. Uchida and M. Watanabe, *Physical Chemistry Chemical Physics*, 2010, 12, 3806-3814.
66. Y. Nabae, M. Sonoda, C. Yamauchi, Y. Hosaka, A. Isoda and T. Aoki, *Catalysis Science & Technology*, 2014, 4, 1400-1406.
67. H. Wang, T. Maiyalagan and X. Wang, *ACS Catal.*, 2012, 2, 781-794.
68. C. V. Rao, C. R. Cabrera and Y. Ishikawa, *The Journal of Physical Chemistry Letters*, 2010, 1, 2622-2627.
69. N. P. Subramanian, X. Li, V. Nallathambi, S. P. Kumaraguru, H. Colon-Mercado, G. Wu, J.-W. Lee and B. N. Popov, *J. Power Sources*, 2009, 188, 38-44.
70. G. Liu, X. Li, P. Ganesan and B. N. Popov, *Electrochim. Acta*, 2010, 55, 2853-2858.
71. M. Lefevre and J.-P. Dodelet, *Electrochim. Acta*, 2003, 48, 2749-2760.
72. S. L. Gojković, S. Gupta and R. F. Savinell, *Electrochimica Acta*, 1999, 45, 889-897.
73. U. A. Paulus, T. J. Schmidt, H. A. Gasteiger and R. J. Behm, *Journal of Electroanalytical Chemistry*, 2001, 495, 134-145.
74. E. Claude, T. Addou, J. M. Latour and P. Aldebert, *J. Appl. Electrochem.*, 1998, 28, 57-64.
75. K. L. Hsueh, D. T. Chin and S. Srinivasan, *J. Electroanal. Chem. Interfacial Electrochem.*, 1983, 153, 79-95.
76. N. Alonso-Vante, H. Tributsch and O. Solorza-Feria, *Electrochim. Acta*, 1995, 40, 567-576.
77. F. Jaouen and J.-P. Dodelet, *The Journal of Physical Chemistry C*, 2009, 113, 15422-15432.
78. N. M. Marković, R. R. Adžić, B. D. Cahan and E. B. Yeager, *Journal of Electroanalytical Chemistry*, 1994, 377, 249-259.
79. V. Stamenković, T. J. Schmidt, P. N. Ross and N. M. Marković, *Journal of Electroanalytical Chemistry*, 2003, 554–555, 191-199.
80. N. Wakabayashi, M. Takeichi, M. Itagaki, H. Uchida and M. Watanabe, *Journal of Electroanalytical Chemistry*, 2005, 574, 339-346.

81. Y. Li, W. Zhou, H. Wang, L. Xie, Y. Liang, F. Wei, J.-C. Idrobo, S. J. Pennycook and H. Dai, *Nature nanotechnology*, 2012, 7, 394-400.
82. X. Li, G. Liu and B. N. Popov, *J. Power Sources*, 2010, 195, 6373-6378.
83. D. Geng, Y. Chen, Y. Chen, Y. Li, R. Li, X. Sun, S. Ye and S. Knights, *Energy Environ. Sci.*, 2011, 4, 760-764.

Figure captions

Figure 1: The chemical structures of the Fe and N sources for Fe/PI and Fe/PI-aw.

Figure 2: Core level N-1s XPS spectra obtained for (A) Fe/PI and (B) Fe/PI-aw. The deconvoluted peaks correspond to pyridinic nitrogen (dark yellow), pyrrolic nitrogen (magenta), graphite-like nitrogen (cyan) and nitrogen oxide (blue) and the overall fitting in each spectrum is shown by red line. Figures C and D correspond to the XPS spectra Fe/PI and Fe/PI-aw after 11,110 cycles of the LD test.

Figure 3: (A) Steady–state voltammograms for the ORR obtained at Fe/PI and Fe/PI-aw catalyst modified GC disk – Pt ring electrode in $O_2$–saturated 0.5 M $H_2SO_4$ solution. The lower panel shows the disk currents and the corresponding Pt ring currents are shown in the upper panel corresponding to the oxidation of $H_2O_2$ produced at the relevant disk electrode. Potential scan rate: 5 mV $s^{-1}$. Electrode rotation speed: 1600 rpm. The Pt ring electrode was potentiostated at 1.2 V. The voltammograms indicated by green lines were obtained at Pt/C-modified GC disk – Pt ring electrode (Pt loading of Pt/C: 55.8 μg $cm^{-2}$) under the same conditions as mentioned above. (B) Variation of the number of electrons ($n$) and $\chi H_2O_2$ with the disk electrode potential during the ORR at the Fe/PI, Fe/PI-aw and Pt/C catalysts.

Figure 4. Comparison of RRDE voltammograms obtained for the ORR at Fe/PI/GC electrode after the each stage of the LD test; before LD test (black), after 10 (red), 110 (green), 1,110 (blue) and 11,110 (cyan) potential-steps. The inset shows the variation of $E_{1/2}$ with the number of the potential-step.

Figure 5: Comparison of individual rate constants ($k_1$, $k_2$ and $k_3$) of the ORR at (A) Fe/PI/GC and (B) Fe/PI-aw/GC electrodes before (solid lines) and after (dashed lines) the LD test. The insets indicate the potential-dependent $k_1/k_2$ values before and after the durability.

Figure 6: Variation of the $H_2O_2$ diffusion-limitted current at 0.2 V vs. Ag/AgCl (sat. KCl) with time elapsed since 10 mM $H_2O_2$ was introduced in $O_2$-saturated 0.1M $HClO_4$ solution containing 2 mg of each catalyst.

Figure 7: Mass transfer – corrected Tafel plots for the ORR at Fe/PI, Fe/PI-aw and Pt/C catalysts.

Figure 1

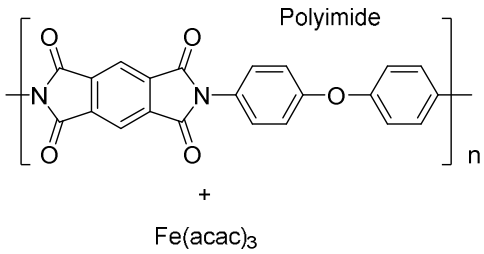

Figure 2

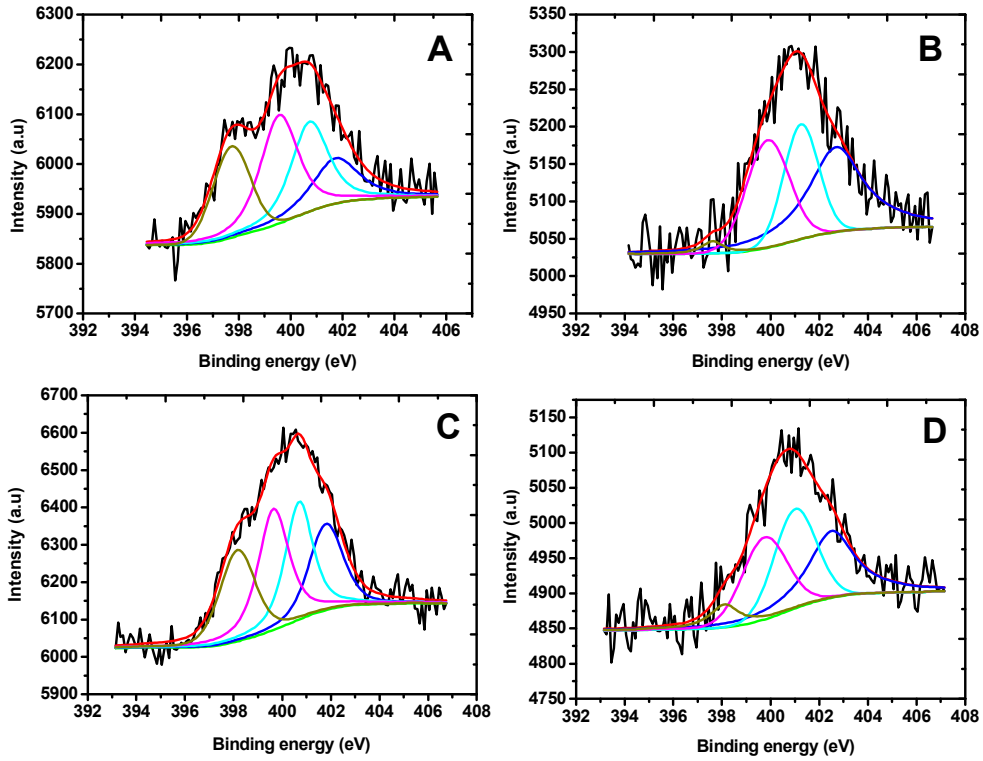

Figure 3

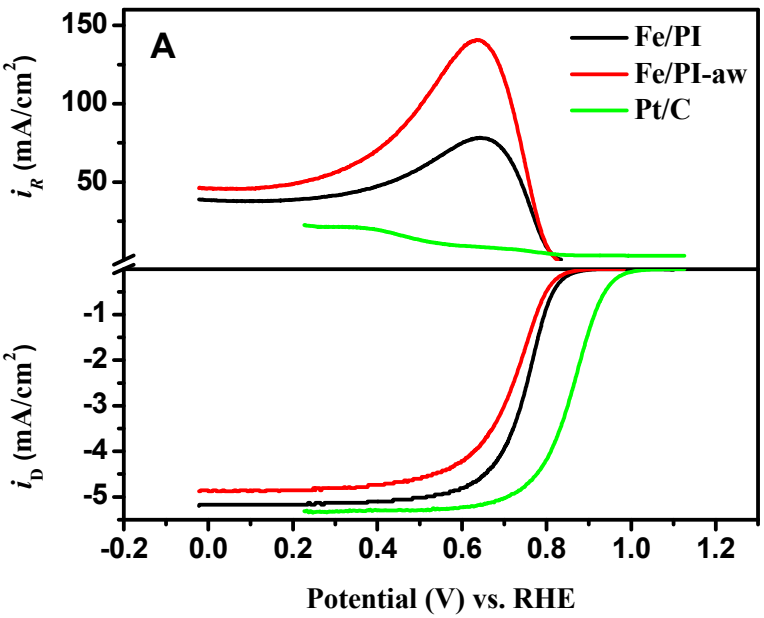


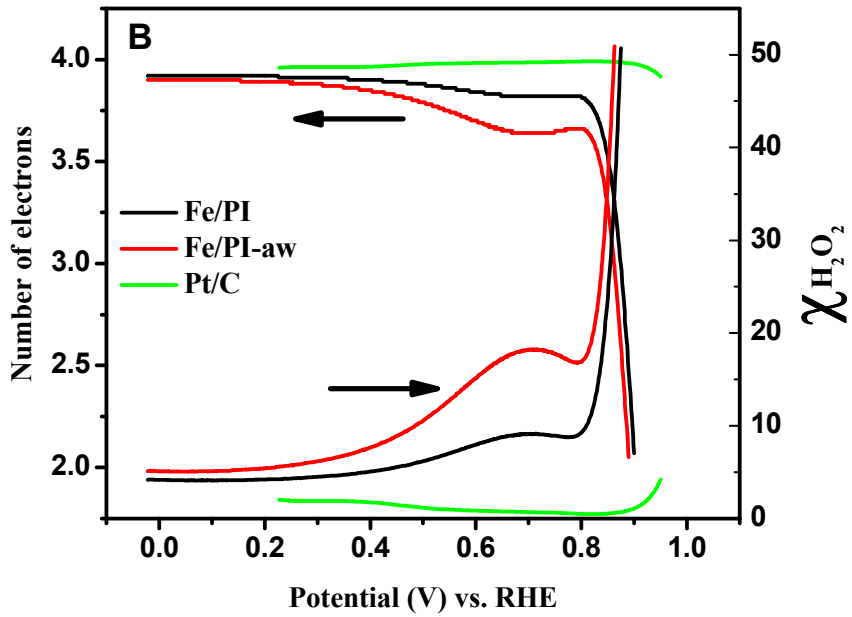

Figure 4

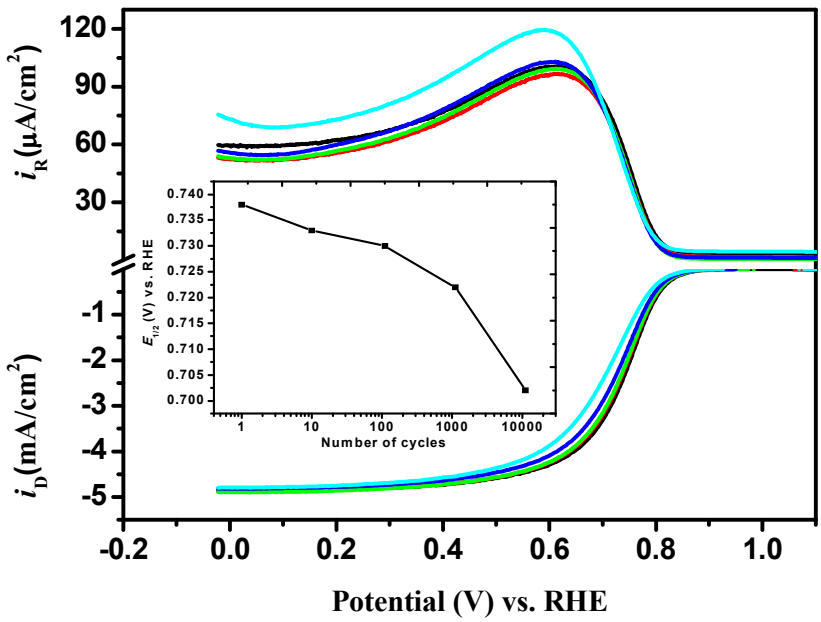

Figure 5

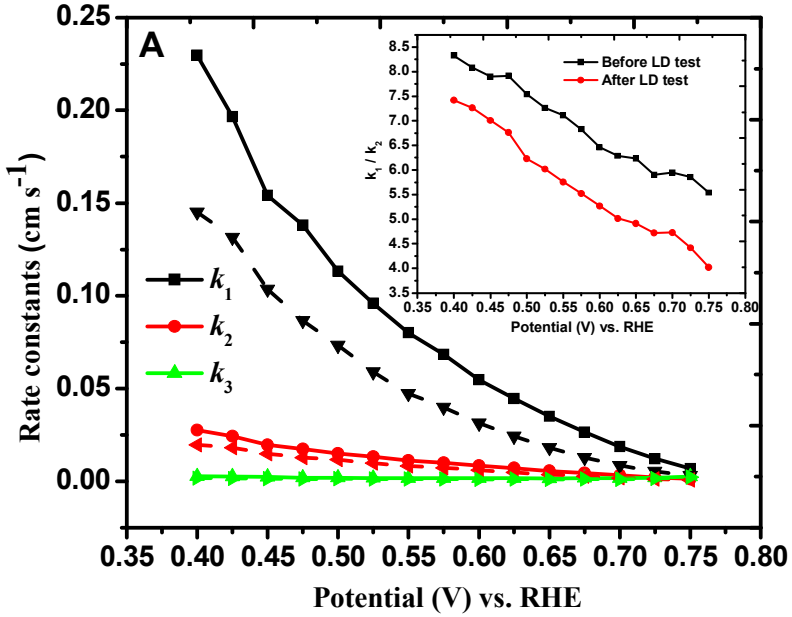


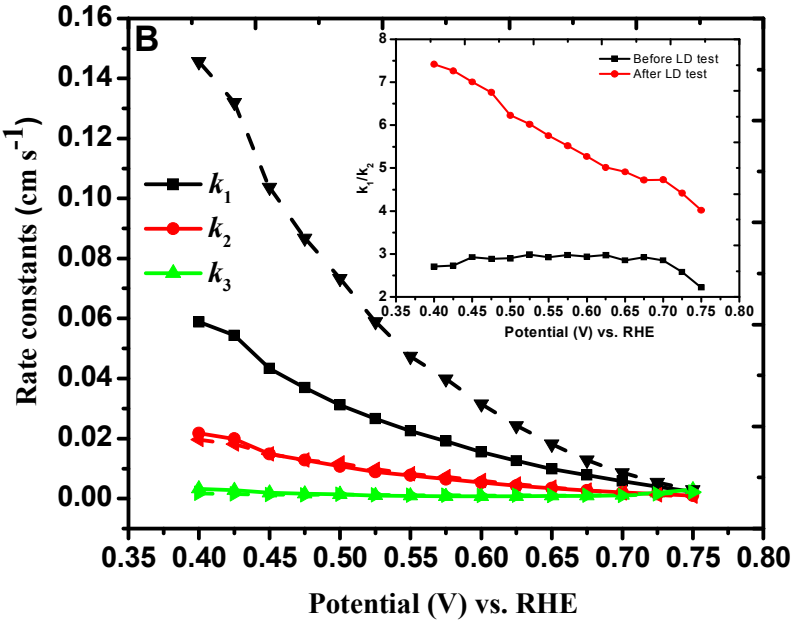

Figure 6

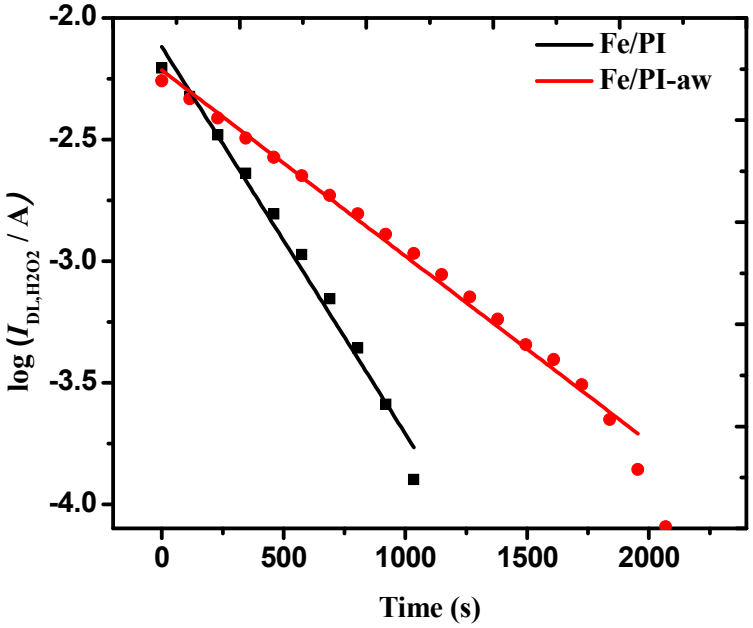

Figure 7

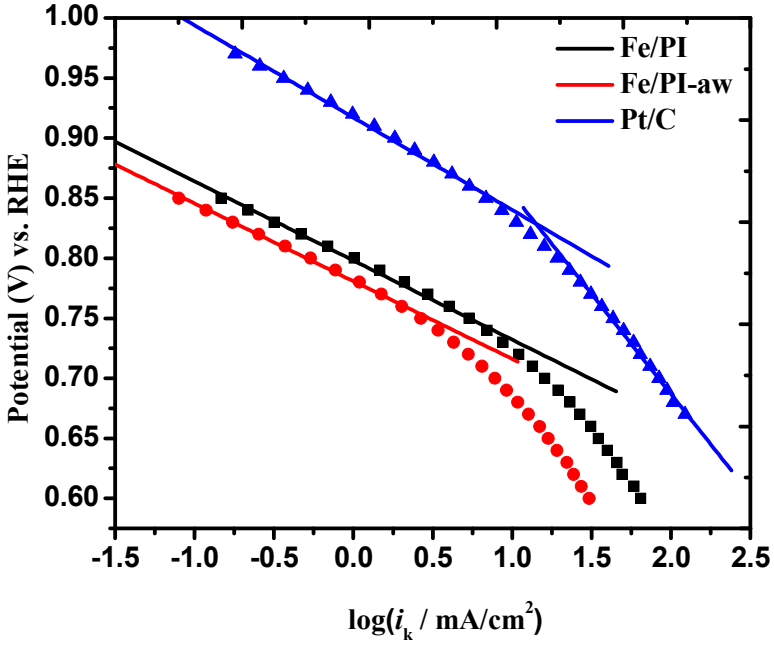

Table 1. Percentages of each kind of nitrogen surface groups in Fe/PI and Fe/PI-aw before and after the LD test (11,110 potential-steps).

| Types of Nitrogen Groups | Fe/PI | | Fe/PI-aw | |
|---|---|---|---|---|
| | Before | After | Before | After |
| Pyridinic | 22 | 23 | 0 | 9 |
| Pyrrolic | 33 | 30 | 31 | 28 |
| Graphite-like | 27 | 26 | 21 | 31 |
| Nitrogen oxide | 18 | 21 | 48 | 32 |

Table 2. Tafel slopes and exchange current densities for the ORR at Fe/PI, Fe/PI-aw and Pt/C.

| Catalysts | Tafel slope (mV $dec^{-1}$) | Exchange current density (A $cm^{-2}$) |
|---|---|---|
| Fe/PI | -66 | $1.1\times10^{-10}$ |
| Fe/PI-aw | -65 | $4.6\times10^{-11}$ |
| Pt/C | -77[a], 167[b] | $3.9\times10^{-8}$ [a], $3.9\times10^{-5}$ [b]. |

[a] lower current density region, [b] higher current density region